Mechanics of some degradation mechanisms in ferroelectric ceramic actuators

M.-Y. He, Zhigang Suo, Robert McMeeking, Anthony Evans, Christopher Lynch

M.-Y. He, Zhigang Suo, Robert M. McMeeking, Anthony G. Evans, Christopher S. Lynch, "Mechanics of some degradation mechanisms in ferroelectric ceramic actuators," Proc. SPIE 2189, Smart Structures and Materials 1994: Smart Materials, (1 May 1994); doi: 10.1117/12.174070

Event: 1994 North American Conference on Smart Structures and Materials, 1994, Orlando, FL, United States

THE MECHANICS OF SOME DEGRADATION MECHANISMS IN FERROELECTRIC CERAMIC ACTUATORS

M.-Y. He, Z. Suo, R.M. McMeeking, A.G. Evans and C.S. Lynch
Mechanical and Environmental Engineering Department
University of California
Santa Barbara, California 93106–5070

ABSTRACT

Several degradation mechanisms in ferroelectric ceramics are analyzed in this article. A ferroelectric crystal under cyclic electric field fatigues by forming a-domain bands. An energy based model is proposed, indicating that these bands are retarded by the electric field, but driven by the shear stress resolved onto the bands. The stress has been attributed to the misfit strain near the 180° domain wall and the edge of the electrodes. A second problem is related to fracture of piezoelectric ceramics. A double-cantilever beam subjected to combined electrical and mechanical loadings is analyzed using finite elements. Also analyzed is electrode debonding, which is shown to decrease capacitance.

1. INTRODUCTION

Ferroelectric ceramics have numerous applications, both existing and potential. One of the more demanding applications is a ferroelectric actuator which functions over a wide range of frequencies. When such actuators operate near the strain and frequency limits of the material, various degradation processes arise. Understanding of these processes is essential for definition of the operational limits of actuators produced from these materials. There are at least two degradation phenomena: breakdown and fatigue. Furthermore, these phenomena occur as the material is subject to cyclic deformation under combined stress and electric field. The phenomena are not well documented and the responsible mechanisms are ill-defined. The intent of the present article is to provide some of the background mechanics needed to address degradation.

Fatigue in ferroelectrics is manifest as a change in the width of the field-polarization hysteresis loop (Fig. 1). There have been various postulates about the mechanism responsible for this effect. It is plausible that more than one mechanism is involved, depending upon the material, the frequency, etc. The mechanisms are in two categories: i) fracture manifests either as microcracking in the ferroelectric or as electrode debonding and, ii) domain wall locking.

Breakdown in multilayer actuators often occurs in association with cracking in the ferroelectric. However, it is not clear whether the crack *precedes* breakdown and provides a breakdown mechanisms, or whether cracking is a *consequence* of breakdown. Some basic results concerning cracks in multilayer ferroelectrics subject to combined stress and electric fields would assist in the development of an understanding about their role in breakdown.

Under cyclic electric field, cracking may take place either in ferroelectric ceramics or along ferroelectric/electrode interface. Cao and Evans (1992) have tested a range of ferroelectrics, antiferroelectrics and relaxors under cyclic electric field of magnitude on the order 1 MV/m. From an indentation flaw introduced prior to testing, cracks grow through the thickness of the sample, in the direction normal to the applied field, at a rate about 1 ~ 100 μm/cycle. The stable cracks grow without macroscopic mechanical loading.

0-8194-1484-0/94/$6.00

With the above background, several calculations are presented which provide a basis for further understanding. The materials of interest are ferroelectric ceramics, such as barium-titanate ($BaTiO_3$) and lead-zirconate-titanate (PZT). Such materials are also piezoelectric. Piezoelectricity is induced by *poling*, wherein the body is subjected to a high electric field which partially aligns the dipoles (Jaffe *et al.*, 1971). Polarization occurs by domain wall motion. Earlier experiments on domain structure and motion (Fatuzzo and Merz, 1967) have indicated that obstacles, developed upon cycling, hinder subsequent domain wall motion. These obstacles represent one potential fatigue mechanism that will be analyzed in this article. The physical nature of the obstacles has not been fully understood.

Ferroelectric ceramics are brittle (toughness, $K_{IC} \approx 1$ MPa$\sqrt{m}$) and susceptible to cracking. Previous studies of cracking have been interpreted on the basis of fracture mechanics concepts with influence of the electric field neglected (Pohanka and Smith, 1987). Recently, a fracture mechanics for ferroelectric ceramics under small-scale nonlinearity conditions has been proposed (Suo *et al.*, 1992). Two problems are examined using this formalism: one concerned with cracks in the ferroelectric and the other with electrode debonding. The notation used in the text and the finite element procedure for calculating piezoelectric fields are summarized in the Appendix.

2. FATIGUE

In this section, one possible fatigue mechanism is explored, using calculations on $BaTiO_3$ to illustrate the effect. Below the Curie temperature (T_c = 120°C), this material is tetragonal, with roughly 1% difference in the *a* and *c* lattice spacings; the polar axis is in the c-direction. Each grain consists of many domains, separated by domain walls (a few lattice spacing thick), which experience jumps in dipole direction. Two types of domain wall exist: 180° walls separate domains having antiparallel dipoles and 90° walls separate domains with perpendicular dipoles. The domain wall is oriented such that the dipole has a continuous normal component, leaving no intrinsic charge on the wall. Thus, 180° walls parallel the c-axis, and 90° walls lie 45° to the c-axis. Further details are documented in Fatuzzo and Merz (1964). One possible fatigue mechanism proposal by Hayashi *et al.* (1964) is illustrated in Fig. 2. A single-domain sample is cycled by an electric field along the c-axis, generating hysteresis curves by 180° domain wall motion. Thin bands of a-domains form within the c-domain and extend upon cycling. These bands apparently hinder 180° wall motion, resulting in fatigue.

2.1 Driving Force

To address the growth of a thin a-domain, both electronic field and shear stresses effect are considered (Fig. 2).* The a-domain is perceived to nucleate at a stress concentration site and then propagate as a thin band across the c-domain. The propagation stage is emphasized in this analysis, leading to an extraction of the critical field E_c needed to cause steady-state extension of a domain having constant width. The shear stress arose from the loads induced during operation of the actuating system, as well as from misfit stress created by domain switching, both upon polarization and during operation.

The critical field is estimated using an energy argument. The stress *facilitates* banding, because unit advance of band decreases the energy by

$$\mathcal{U}_\sigma = -2\gamma_0 \sigma b, \tag{2.2}$$

where $\gamma_0 = (c-a)/a$ is the strain associated with the atom rearrangement in the c-to-a transition, b is the band width, and σ is the shear stress on the band. Conversely, the electric field *retards* banding, because unit advance of the band increases the energy by

* The hydrostatic stress does not contribute to banding.

$$\mathcal{U}_E = P_s E b, \tag{2.1}$$

where P_s is the spontaneous polarization and E the electric field: $\mathcal{U}_E$ has a dimension of surface energy. The net energy release rate is

$$\mathcal{G} = -\left(\mathcal{U}_\sigma + \mathcal{U}_E\right) = 2\gamma_o \sigma b - P_s E b. \tag{2.3}$$

As the band advances, new 90° domain walls are created on the two sides, having energy per unit area, Γ. Consequently, the band advances provided that

$$\mathcal{G} > 2\Gamma, \tag{2.4a}$$

or, more explicitly,

$$2\gamma_o \sigma b - P_s E b > 2\Gamma \tag{2.4b}$$

such that

$$E_c = 2\left(\gamma_o \sigma b - \Gamma\right)/P_s b \tag{2.4c}$$

A numerical estimate for $BaTiO_3$ provides perspective. The thickness of bands found experimentally is, b = 1 μm (Hayashi *et al.* 1964). The tetragonality at room temperature is c = 4.026 Å, a = 3.987 Å, so that $\gamma_0 = 0.01$. The spontaneous polarization for $BaTiO_3$ is $P_s = 0.26\ C/m^2$. The domain wall energy is $\Gamma = 0.01\ Jm^{-2}$. With E = 0.5 MV/m, $\mathcal{U}_E = 0.13\ J/m^2$.

As will be shown in the next subsection, the induced stress is often linear with the applied electric field, i.e., $\sigma = f e_{33} E$, where f is a dimensionless number and e_{33} is piezoelectric constant (see Table I). Consequently, Eqn. ((2.4) can be rewritten as

$$E > 2\Gamma/b\left(2f\gamma_o e_{33} - P_s\right). \tag{2.5}$$

Thus, a critical field exists, below which the bands will not form.

Similar bands form when an electric field is applied perpendicular to the c-axis (Zheludev 1971). With the stress ignored, the field needed for banding is given by

$$E > 2\Gamma/b P_s. \tag{2.6}$$

Actuators are typically subjected to mechanical load. The stress on the order of 10 MPa can be easily generated from the load. Stress can be induced even without applied mechanical load. One case, illustrated in Fig. 3, is analyzed using finite elements.

The 180° domain wall is a stress concentration site (Fig. 3a). Note that, when the voltage is applied, due to piezoelectricity, the domain on the left shrinks, but that on the right expands. Each domain is taken to be linearly piezoelectric, with physical constants given in Table I. It is known that the physical constants are different between a single domain and a poled ceramic, but stresses computed below are not very sensitive to such differences. Contours of normal stress σ_{33} (Fig. 4b) indicate that this stress is tensile on the left and compressive on the right, reaching a maximum along the wall.

Let (r, θ) be the polar coordinates centered at the bottom wall-surface intersection. The stresses near the intersection should not feel the existence of the top surface, so that the only length involved is r. Dimensionality and linearity dictate that the stresses near the intersection take the form

$$\sigma_{ij} = f_{ij}(\theta) e_{33} V/h \tag{2.7}$$

with the dimensionless coefficient f dependent on θ and physical constants. The near-intersection distributions (Fig. 4) indicate that σ_{rr} and $\sigma_{r\theta}$ reach the maximum at the wall, but σ_{θ} reaches its maximum at $\theta = 57°$. In $BaTiO_3$ with $e_{33} = 18.6\ C/m^2$, for $V/h = 0.5\ MV/m$, the stress along the domain boundary is estimated to be

$$\sigma_{rr}\left(\theta = 90°\right) = \sigma_{zz} \cong 1.2 e_{33} v/h \cong 11 MPa. \tag{2.8}$$

Judged from Eqn. (2.4b), the magnitude is close to that needed to drive a band.

3. CRACKING AND DEBONDING

A set of experiments on ferroelectric ceramics has been conducted (Cao and Evans 1992), using specimens illustrated in Fig. 5, under a cyclic electric field (M = 0, V is cyclic). The crack grows stably with the cycle, mimicking crack growth in metals under cyclic mechanical loading.

Non-uniform, irreversible strains associated with ferroelectric twinning must be present at the crack tip, caused by the intensified electric field. Such strains can cause stresses of magnitude $\sigma \sim C_{11}\gamma_0 = 1\ GPa$, which is localized near the crack tip. It is speculated that this high-magnitude, localized stress drives the crack growth in the brittle ceramics. Detailed modelling will not be pursued in this paper. Instead, a linear fracture mechanics approach is described in the following sections.

3.1 Crack Tip Field

Suo *et al.* (1992) have formulated a fracture mechanics for ferroelectrics under combined stress and electric field. The theory is phenomenological and applies when the material is linearly piezoelectric, except for a small nonlinear zone around the crack tip. In this paper, we assume that the cracks are impermeable, such that $D_z = 0$ applies on the crack surfaces, where D is the electric induction. However, it is noted that, under certain conditions, cracks can conduct electricity (McMeeking 1987, 1990 and Suo 1992).

Stress and electric induction are square root singular around a crack tip. For a planar crack, with its front perpendicular to the poling axis, under in-plane mechanical and electrical loading (Fig. 5), three types of intensity factors can be induced, K_I, K_{II} and K_{IV}. They are defined such that at a distance r ahead of the crack tip

$$\sigma_{zz} = \frac{K_I}{\sqrt{2\pi r}}, \quad \sigma_{xz} = \frac{K_{II}}{\sqrt{2\pi r}}, \quad D_z = \frac{K_{IV}}{\sqrt{2\pi r}}. \tag{3.1}$$

The jumps in displacements and electric potential at a distance r behind the crack tip are

$$\left[\Delta u_x,\ \Delta u_z,\ \Delta\phi\right]^T = \left(2r/\pi\right)^{1/2} H\left[K_{II},\ K_I,\ K_{IV}\right]^T, \tag{3.2}$$

where H is a real, symmetric matrix. The relation connecting the energy release rate, $\mathcal{G}$, and the intensity factors, K, is quadratic,

$$\mathcal{G} = \frac{1}{4}\left[K_{II},\ K_I,\ K_{IV}\right] H \left[K_{II},\ K_I,\ K_{IV}\right]^T. \tag{3.3}$$

When the crack plane is normal to the poling axis, H takes the form

$$\frac{1}{4}H = \begin{bmatrix} \frac{1}{c_L} & 0 & 0 \\ 0 & \frac{1}{c_T} & \frac{1}{e} \\ 0 & \frac{1}{e} & -\frac{1}{\varepsilon} \end{bmatrix}, \tag{3.4}$$

where c_L and c_T have the dimensions of elasticity, ε permitivity and e piezoelectricity. Note that $\mathcal{G}$ due to K_{IV} is negative. A numerical procedure described in Suo *et al.* (1992) may be used to compute these constants, but a different procedure is used here, described below.

3.2 Cracking

For a crack of length 2a in an infinite piezoelectric, subject to a uniform remote field $\{\sigma^{\infty}_{zz}, \sigma^{\infty}_{xz}, D^{\infty}_{z}\}$, the intensity factors are

$$[K_{II}, K_I, K_{IV}] = \sqrt{\pi a}\,[\sigma^{\infty}_{xz}, \sigma^{\infty}_{zz}, D^{\infty}_{z}]. \tag{3.5}$$

Finite elements are used to compute the energy release rate, whereby the J-integral is evaluated for several far field combinations. The known solution (Eqn. 3.5), together with Eqn. (3.3), allows the constants in H to be computed. The results are

$$BaTiO_3: c_L = 0.804\,c_{33},\quad c_T = 0.877\,c_{33},\quad e = 12.6\,e_{33},\quad \varepsilon = 1.64\,\varepsilon_{33}, \tag{3.6}$$

and

$$PZT:\ c_L = 0.850 c_{33},\ c_T = 0.847 c_{33},\ e = 9.35 e_{33},\ \varepsilon = 2.84\,\varepsilon_{33}. \tag{3.7}$$

The effects of finite geometry are illustrated using the configuration depicted in Fig. 5, subject to applied moments, M, and a voltage, V. The top and bottom surfaces are electroded, but traction-free. By dimensional considerations, the intensity factors have the functional forms

$$K_I = k_{11} M h^{-3/2} + k_{14} e_{33} V h^{-1/2}, \tag{3.8}$$

$$K_{IV} = k_{41} (\varepsilon_{33}/c_{33})^{1/2} M h^{-3/2} + k_{44} \varepsilon_{33} V h^{-1/2}, \tag{3.9}$$

where the dimensionless coefficients k depend on material constants. The finite element results are

$$BaTiO_3:\ k_{11} = 5.14,\ k_{14} = -0.1,\ k_{41} = 2.19,\ k_{44} = 1.01, \tag{3.10}$$

and

$$PZT:\ k_{11} = 4.64,\ k_{14} = 0.05,\ k_{41} = 3.49,\ k_{44} = 1.41. \tag{3.11}$$

In the finite element calculation, two loading cases, M and V, are solved independently. For each case, the jumps across the crack, Δu_z and $\Delta\phi$, are computed near the crack tip, and K_I and K_{IV} are inferred from Eqn. (3.2).

The voltage V alone induces a K_I, which is typically small. For example, for $BaTiO_3$ with V/h = 1 MV/m and h = 1 mm, Eqn. (3.8) gives $K_I = -0.07$ MPa $m^{1/2}$. This magnitude is negligible compared with the ceramic toughness. Similarly, the K_{IV} induced by bending moments alone is also small.

The fact that the voltage contributes little to K_I does not imply, however, that the electric field does not affect the fracture process. The electric field concentrated at the crack tip switches the poling direction at the crack tip, which induces large strain and stress as discussed previously. These details cannot be captured by the linear fracture mechanics. Nonetheless, under the condition that the nonlinear zone is small compared with the specimen size, experimentally, one can correlate the failure loci of (K_I, K_{VI}) measured from different specimens. The concept is analogous to using (K_I, K_{II}) to correlate mixed-mode fracture of elastic-plastic materials under small-scale yielding conditions. It is also possible to correlate crack growth rate with the magnitude of K_{IV} under cyclic electric loading, a procedure similar to that for metal fatigue crack under cyclic mechanical loading.

3.3 Electrode Debonding

Electrode debonding is a potential failure mode in ferroelectric actuators. Fig. 6 illustrates a representative geometry; PZT is used in calculation. When the debond length exceeds a fraction of the ceramic thickness, the energy release rate, $\mathcal{G}$, must approach an asymptotic value, $\mathcal{G}_{ss}$, independent of the debond length. To evaluate $\mathcal{G}_{ss}$, it is noted that the wake, far behind the debond tip, is free from loading, whereas ahead of the crack tip, the only non-zero component of the electric field is

$$E_3 = V/h. \tag{3.12}$$

The steady-state $\mathcal{G}$ is thus,

$$\mathcal{G}_{ss} = -\varepsilon_{33}^{\sigma} V^2/4h, \tag{3.13}$$

where the stress-free permitivity ε^{σ} is used. (Note that there are two cracks.) Results for short cracks (a/b = 0.1 ~ 0.5) are analyzed using finite elements, as plotted in Fig. 7a. As the debond extends, the capacitance, C, must decrease. An analog to the linear elastic calculation dictates that C be related to $\mathcal{G}$ by

$$\mathcal{G} = \frac{1}{2} V^2 (\partial C/\partial A). \tag{3.14}$$

This relation is analogous to the Irwin-Kies relation in fracture mechanics. A more general version is given in Suo (1991). Consequently, as the debond area increases from A_0 to A, the capacitance changes by

$$C(A) - C(A_0) = \frac{2}{V^2} \int_{A_0}^{A} \mathcal{G}\, dA. \tag{3.15}$$

Fig. 7b plots the capacitance decrease.

Contours of constant stress σ_{33} are shown in Fig. 8 for a/b = 0.2. The crack tip stress distribution is shown in Fig. 9. These results show that the stresses induced by the voltage are singular at the crack tip, but the stress intensity factors are relatively small. The structure of the near tip field for such an interface crack is complicated, as shown in Suo *et al.* (1992). No effort has been given to evaluate precise value of

the intensity factors. For a typical field, $V/h = 1$ MV/m and thickness, $h = 1$ mm, the maximum normal stress near the crack, at $r/a = 0.002$ is $\sigma_r \approx 6$ MPa.

4. CONCLUDING REMARKS

Ferroelectric single crystals are susceptible to a-domain bands driven by shear stress. The stress can be induced by mechanical load or mismatch strains near the domain walls. For cracks in multilayer actuators, K_I due to the voltage is small and K_{IV} gives a negative energy release rate. Under static electric loading, the actuators are unlikely to fracture. Cyclic loading causes the crack tip to undergo repeated depoling and hysteresis, which may lead to slow crack growth. In this article, we have assumed cracks to be impermeable. In practice, a crack can conduct electricity if charged species are available on the crack surfaces. Conducting cracks perpendicular to electrodes can grow under combined stress and electric field, leading to electrical short.

5. REFERENCES

Cao, H.C. and Evans, A.G., (1992), Electric field induced fatigue crack extension in ferroelectric ceramics, manuscript in preparation.

Fatuzzo, E. and Merz, W. J. (1967), *Ferroelectricity*, North Holland, New York.

Hayashi, M., Imaizumi, S. and Abe, R. (1964), Decay of switching current in switching of $BaTiO_3$ crystal due to a-domain formation, *Japanese J. Appl. Phys.*, **3**, 637–643.

Jaffe, B., Cook, W. R. and Jaffe, H. (1971), *Piezoelectric Ceramics*, Academic Press, New York.

McMeeking, R. M. (1987), On mechanical stresses at cracks in dielectrics with application to dielectric breakdown, *J. Appl. Phys.*, **62**, 3116–3122.

McMeeking, R. M. (1990), A J-integral for the analysis of electrically induced mechanical stress at cracks in elastic dielectrics, *Int. J. Eng. Sci.*, **28**, 605–613.

Pohanka, R. C. and Smith, P. L. (1987), Recent advances in piezoelectric ceramics, in *Electronic Ceramics*, ed. L. M. Levinson, pp. 45–146, Marcel Dekker, Inc., New York.

Suo, Z., Kuo, C.-M., Barnett, D. M. and Willis, J. R. (1992), Fracture mechanics for piezoelectric ceramics, *J. Mech. Phys. Solids*, **40**, 739–765.

Suo, Z. (1992) Models for breakdown-resistant dielectric and ferroelectric ceramics, submitted for publication.

Suo, Z. (1991) Mechanics concepts for failure in ferroelectric ceramics. In *Smart Structure and Materials*, Ed. A.V. Srinvasan, pp. 1–6, ASME, New York.

Zheludev, I. S. (1971), *Physics of Crystalline Dielectrics*, p. 420, Plenum Press, New York.

APPENDIX

The strain γ and the electric field $\mathbf{E}$ are derived from the displacement field $\mathbf{u}$ and the electric potential field ϕ by

$$\gamma_{ij} = \frac{1}{2}\left(u_{i,j} + u_{j,i}\right), \quad E_i = -\phi_{,i}. \tag{A.1}$$

The stress σ and the electric induction $\mathbf{D}$ are divergence free, i.e.,

$$\sigma_{ij,i} = 0, \quad D_{i,i} = 0. \tag{A.2}$$

Here the external body force and bulk charge are taken to be negligible. The constitutive relations for linear piezoelectrics are

$$\sigma_{ij} = C_{ijrs}\gamma_{rs} - e_{sij}E_s, \quad D_i = \varepsilon_{is}E_s + e_{irs}\gamma_{rs}. \tag{A.3}$$

where C is the elasticity, ε the permitivity and e the piezoelectricity.

The mechanical boundary conditions are taken to be

$$n_i\sigma_{ij} = t_j^0, \quad \text{on } s_t, \tag{A.4a}$$

$$u_j = u_j^0, \quad \text{on } s_u, \tag{A.4b}$$

where the superscript 0 indicates the prescribed values. The electric boundary conditions are

$$n_i D_i = -\omega^0, \quad \text{on } s_\omega, \tag{A.5a}$$

$$\phi = \phi^0, \quad \text{on } s_\phi, \tag{A.5b}$$

In the above, the stress and the electric induction in the environment are assumed to be negligible.

A finite element procedure can be formulated using the variational principle by defining a functional

$$\Omega(u,\phi) = \int_v \left[\frac{1}{2} C_{ijrs} u_{j,i} u_{r,s} - \frac{1}{2} \varepsilon_{is} \phi_{,i} \phi_{,s} + e_{irs} \phi_{,i} u_{r,s}\right] dv - \int_{s_t} t_j^0 u_j ds - \int_{s_\omega} \omega^0 \phi ds, \tag{A.6}$$

where (u, ϕ) satisfies Eqns. (A.4b) and (A.5b). The solution satisfies

$$\delta\Omega = 0. \tag{A.7}$$

The finite elements have four degrees of freedom, u_1, u_2, u_3 and ϕ, at each node. Since the energy function is not positive definite, the solution need not minimize Ω.

For poled ferroelectrics, the constitutive equation has transverse symmetry around the poling axis (axis-3):

$$\begin{bmatrix}\sigma_{11}\\ \sigma_{22}\\ \sigma_{33}\\ \sigma_{23}\\ \sigma_{13}\\ \sigma_{12}\end{bmatrix} = \begin{bmatrix} c_{11} & c_{12} & c_{13} & 0 & 0 & 0 \\ c_{12} & c_{11} & c_{13} & 0 & 0 & 0 \\ c_{13} & c_{13} & c_{33} & 0 & 0 & 0 \\ 0 & 0 & 0 & c_{44} & 0 & 0 \\ 0 & 0 & 0 & 0 & c_{44} & 0 \\ 0 & 0 & 0 & 0 & 0 & \frac{1}{2}(c_{11}-c_{12}) \end{bmatrix} \begin{bmatrix}\gamma_{11}\\ \gamma_{22}\\ \gamma_{33}\\ 2\gamma_{23}\\ 2\gamma_{13}\\ 2\gamma_{12}\end{bmatrix} - \begin{bmatrix} 0 & 0 & e_{31} \\ 0 & 0 & e_{31} \\ 0 & 0 & e_{33} \\ 0 & e_{15} & 0 \\ e_{15} & 0 & 0 \\ 0 & 0 & 0 \end{bmatrix} \begin{bmatrix}E_1\\ E_2\\ E_3\end{bmatrix}, \tag{A.8}$$

$$\begin{bmatrix}D_1\\ D_2\\ D_3\end{bmatrix} = \begin{bmatrix} 0 & 0 & 0 & 0 & e_{15} & 0 \\ 0 & 0 & 0 & e_{15} & 0 & 0 \\ e_{31} & e_{31} & e_{33} & 0 & 0 & 0 \end{bmatrix} \begin{bmatrix}\gamma_{11}\\ \gamma_{22}\\ \gamma_{33}\\ 2\gamma_{23}\\ 2\gamma_{13}\\ 2\gamma_{12}\end{bmatrix} + \begin{bmatrix} \varepsilon_{11} & 0 & 0 \\ 0 & \varepsilon_{11} & 0 \\ 0 & 0 & \varepsilon_{33} \end{bmatrix} \begin{bmatrix}E_1\\ E_2\\ E_3\end{bmatrix}. \tag{A.9}$$

Poled $BaTiO_3$ and PZT have been selected in the finite element calculations because both have been extensively studied and their physical constants well documented (Jaffe *et al.* 1971) (Table 1).

Now consider the plane problems in the (1, 3)-plane: nothing varies with x_2. For a problem involving a length h and an applied stress σ_0, all the quantities may be normalized as

$$\bar{\sigma} = \sigma/\sigma_0, \quad \bar{D} = D(c_{33}/\varepsilon_{33})^{1/2}/\sigma_0, \quad \bar{\phi} = \phi(c_{33}\varepsilon_{33})^{1/2}/\sigma_0 h, \quad \bar{u} = uc_{33}/\sigma_0 h,$$

$$\bar{c} = c/c_{33}, \quad \bar{e} = e/(c_{33}\varepsilon_{33})^{1/2}, \quad \bar{\varepsilon} = \varepsilon/\varepsilon_{33}, \quad \bar{x} = x/h. \tag{A.10}$$

The constitutive equations can be rewritten as

$$\begin{bmatrix}\bar{\sigma}_{11}\\ \bar{\sigma}_{33}\\ \bar{\sigma}_{13}\\ \bar{D}_1\\ \bar{D}_3\end{bmatrix} = \begin{bmatrix} \bar{c}_{11} & \bar{c}_{13} & 0 & 0 & \bar{e}_{31} \\ \bar{c}_{13} & \bar{c}_{33} & 0 & 0 & \bar{e}_{33} \\ 0 & 0 & \bar{c}_{44} & \bar{e}_{15} & 0 \\ 0 & 0 & \bar{e}_{15} & -\bar{\varepsilon}_{11} & 0 \\ \bar{e}_{31} & \bar{e}_{33} & 0 & 0 & -\bar{\varepsilon}_{33} \end{bmatrix} \begin{bmatrix} \bar{u}_{1,1} \\ \bar{u}_{3,3} \\ \bar{u}_{1,3} + \bar{u}_{3,1} \\ \bar{\phi}_{,1} \\ \bar{\phi}_{,3} \end{bmatrix}, \tag{A.11}$$

The analogy between anti-plane displacement u_2 and electric potential ϕ is obvious. The piezoelectric problem is therefore the same as an elastic problem containing both in-plane and anti-plane displacements. Thus, a general purpose finite element code, ABAQUS, was modified to calculate the piezoelectric field.

TABLE 1

Material Constants of Barium-Titanate ($BaTiO_3$) and Lead-Zirconate-Titanate (PZT)

Material		$BaTiO_3$	PZT
Elastic Constants (GPa)	c_{11}	166	139
	c_{12}	76.6	77.8
	c_{13}	77.5	74.3
	c_{33}	162	115
	c_{66}	44.8	25.6
Piezoelectric Constants (C/m^2)	e_{31}	−4.4	−5.5
	e_{33}	18.6	15.1
	e_{15}	11.6	12.7
Dielectric Constants $\varepsilon_0 = 8.854$ pF/m	ε_{11}	$1620\varepsilon_0$	$1475\varepsilon_0$
	ε_{33}	$1900\varepsilon_0$	$1300\varepsilon_0$

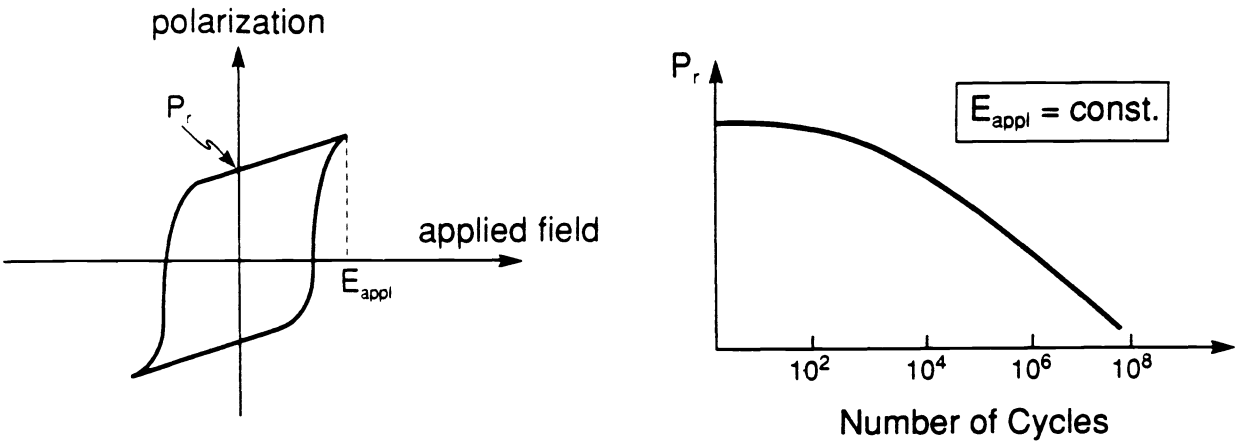

Fig. 1. Changes in the hysteresis loop for a ferroelectric ceramic subjected to cyclic electric field.

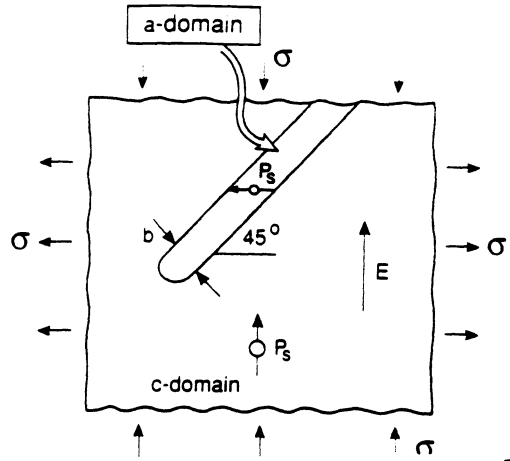

Fig. 2. A schematic of an a-domain band forming at the intersection of a 180° domain with a surface.

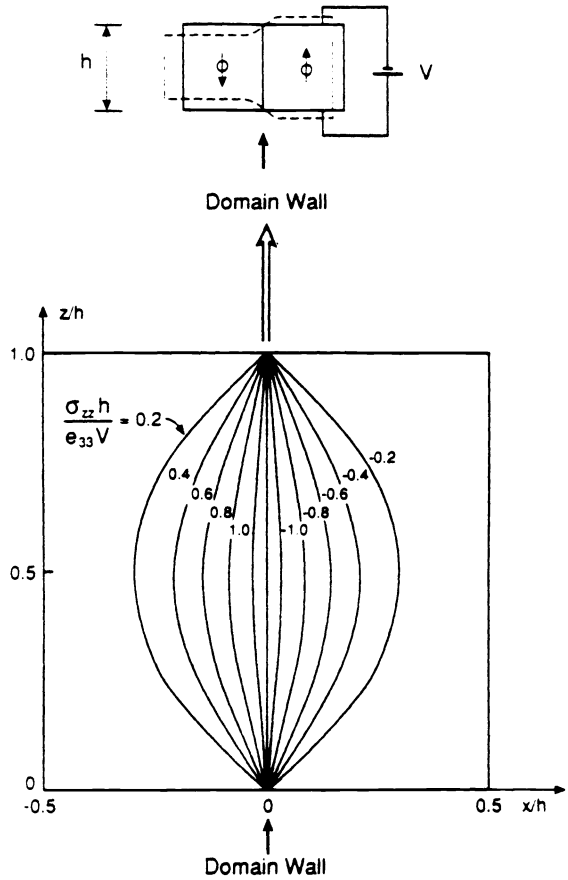

Fig. 3. Contours of the dimensionless normal stress $\sigma_{33}h/e_{33}V$.

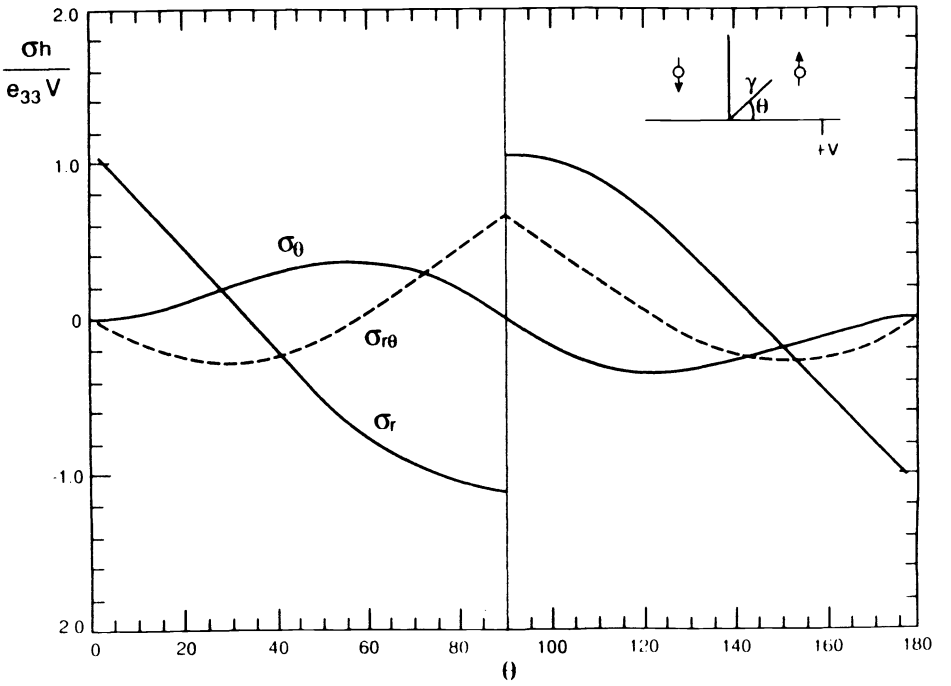

Fig. 4. Stress distribution around the intersection between and 180° domain wall and the sample surface.

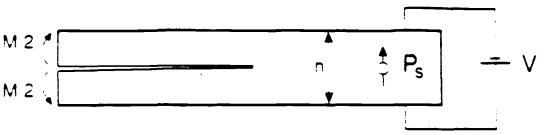

Fig. 5. A double-cantilever-beam subjected to moments and voltage; the crack front is perpendicular to the poling axis.

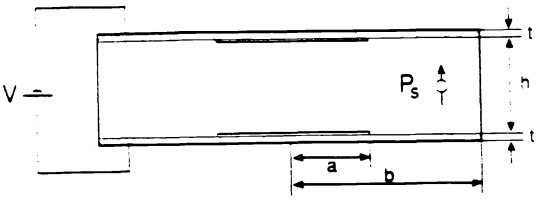

Fig. 6. Electrode debonding.

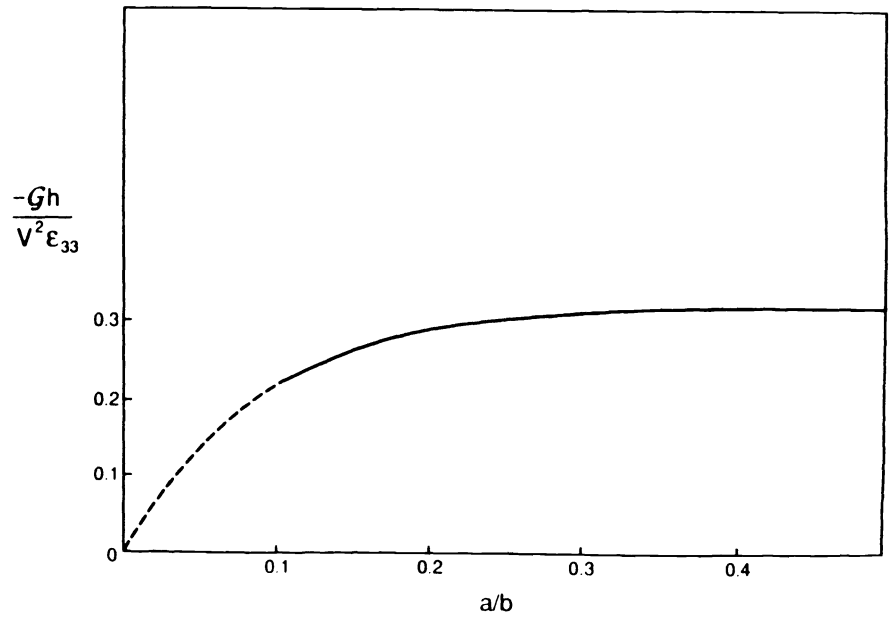

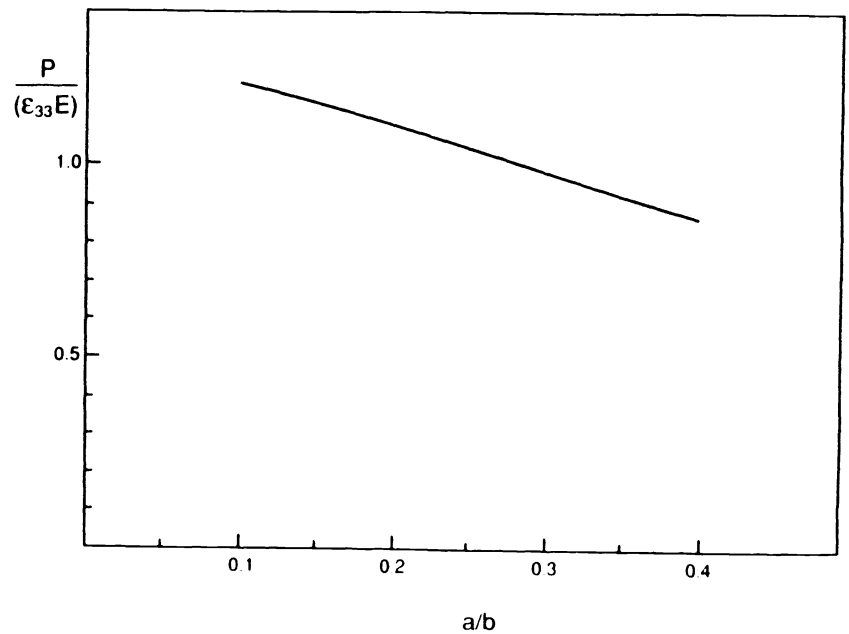

Fig. 7. a) Energy release rate. b) Capacitance.

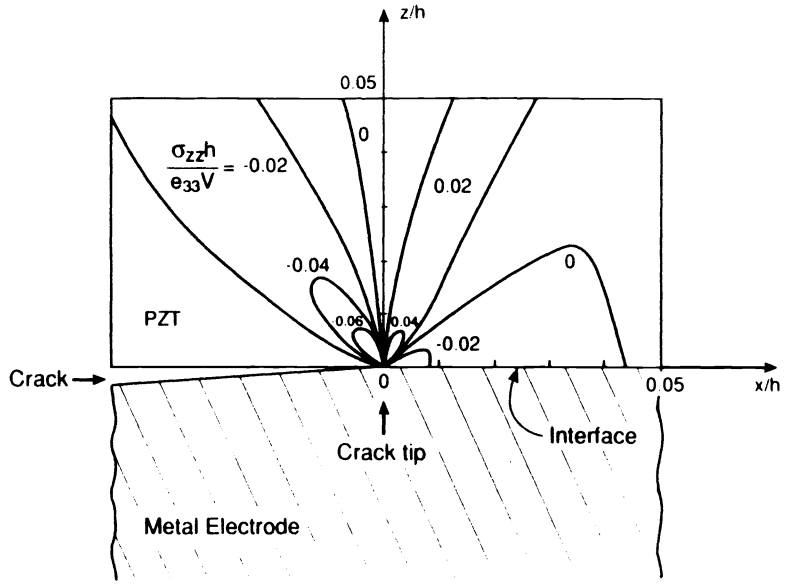

Fig. 8. Contours of the normalized normal stress $\sigma_{33}h/e_{33}V$ around a crack on the electrode/ceramic interface.

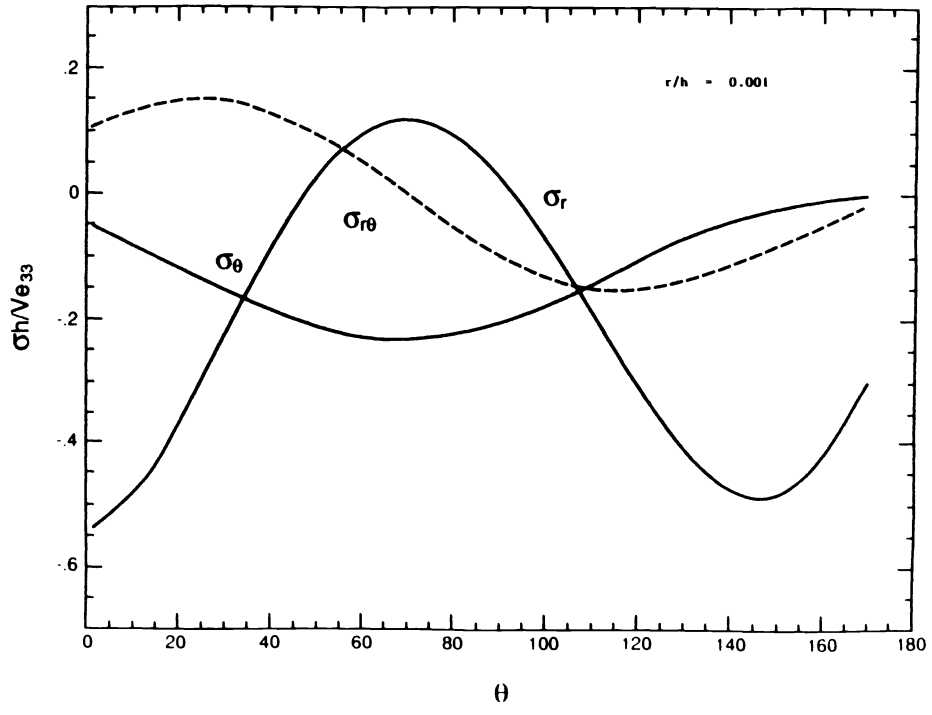

Fig. 9. Near-tip stress distribution.